BILKENT UNIVERSITY
DEPARTMENT OF ELECTRICAL AND ELECTRONICS ENGINEERING

EEE 492 – SENIOR PROJECT
FINAL REPORT

Interference and Noise Robust Image Reconstruction for Magnetic Particle Imaging

Berfin Kavşut
21602459

Abstract

Magnetic Particle Imaging (MPI) is a recently introduced medical imaging modality using the nonlinear magnetization response of superparamagnetic iron oxide (SPIO) nanoparticles. Partial field-of-view Center Imaging (PCI) is a novel robust x-space image reconstruction for MPI developed with the motivation of eliminating non-ideal effects on the signal. PCI and Lumped-PCI methods offer a trade-off between interference and noise robustness. PCI offers robustness against harmonic interferences, whereas Lumped PCI offers robustness against noise. This project aims to develop an image reconstruction technique for MPI that simultaneously improves interference and noise robustness, effectively combining PCI and Lumped-PCI in an optimized fashion.

December 27, 2020

Interference and Noise Robust Image Reconstruction for Magnetic Particle Imaging

1. Background

1.1. X-Space Reconstruction

Magnetic Particle Imaging (MPI) is a new tomographic imaging modality using the nonlinear magnetization response of superparamagnetic iron oxide (SPIO) nanoparticles. Permanent magnetic field called as selection field creates field free point (FFP). FFP is moved by sinusoidal excitation field to scan field-of-view (FOV). Due to safety limitations in MPI, FOV is divided into partial field-of-views (pFOV). FFP, which was created by the selection field, is moved by applying an additional focus field to be able to cover whole FOV without violating safety limitations. Alternatively, phantom can be moved mechanically [1].

In x-space reconstruction, received signal is gridded and speed-compensated in pFOVs, and then pFOVs are combined to obtain whole image in FOV. $\rho(x)$ is the particle distribution, $h(x)$ is the point spread function (PSF), $x_s(t)$ is the instantaneous FFP position, $\hat{\rho}(x)$ is PSF blurred ideal MPI image, $s(t)$ is received signal, $\dot{x_s}(t)$ is the instantaneous FFP speed and γ is a constant including information such as magnetic particle features [1].

$$s(t) = \gamma \dot{x_s}(t) \hat{\rho}(x_s(t)) \tag{1}$$

$$\hat{\rho}\big(x_s(t)\big) = \frac{s(t)}{\gamma \dot{x_s}(t)} \tag{2}$$

$$\hat{\rho}(x_s(t)) = \rho(x) * h(x)\big|_{\,x = x_s(t)} \tag{3}$$

As seen in Eqn. 2, PSF blurred image can be obtained by dividing received signal with instantaneous FFP speed. Excitation signal is chosen to be sinusoidal, and therefore $s(t)$ is a periodic signal. f_0 is the fundamental frequency of signal, which is the frequency of excitation field, and S_n's are Fourier coefficients of $s(t)$ in Eqn 4.

$$s(t) = \sum_{n=1}^{\infty} S_n \sin(2\pi n f_0 t) \tag{4}$$

$x_s(t) = W\cos(2\pi f_0 t)$, where W is the width of pFOV. When speed compensation is applied on each harmonic signal of $s(t)$, MPI harmonic image basis set becomes linear combination of Chebyshev polynomials of the second kind U_{n-1}'s weighted by Fourier coefficients S_n's as shown in Eqn. 5 [2].

$$\begin{aligned}\hat{\rho}(x) &= \left.\frac{s(t)}{\gamma \dot{x}_s(t)}\right|_{t=\frac{1}{(2\pi f_0)}\arccos\left(\frac{2x}{W}\right)} \\ &= \sum_{n=1}^{\infty} S_n \left.\frac{\sin(2\pi n f_0 t)}{\sin(2\pi f_0 t)}\right| t = \frac{1}{(2\pi f_0)}\arccos\left(\frac{2x}{W}\right) \\ &= \sum_{n=1}^{\infty} S_n \frac{\sin\left(\pi \arccos\left(\frac{2x}{W}\right)\right)}{\sin\left(\arccos\left(\frac{2x}{W}\right)\right)} \\ &= \sum_{n=1}^{\infty} S_n U_{n-1}\left(\frac{2x}{W}\right)\end{aligned} \tag{5}$$

Here, Chebyhev polynomials of second kind are displayed separately in Figure 1.

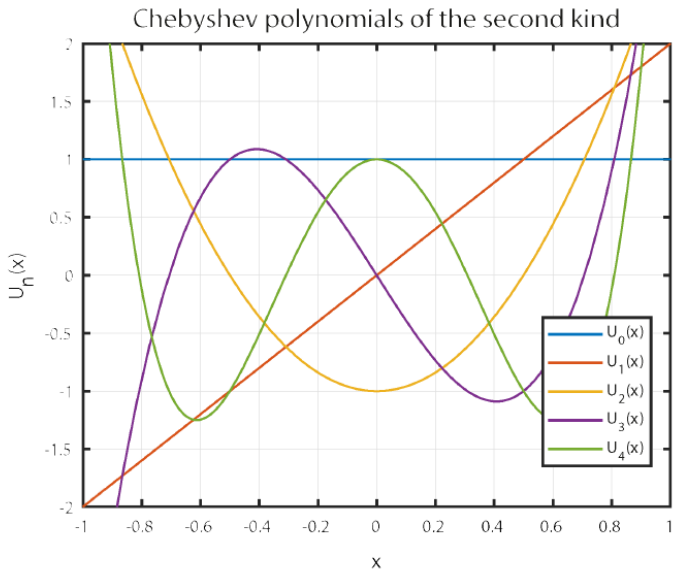

Fig. 1: Chebyshev Polynomials of the Second Kind [3]

In MPI, first harmonic signal cannot be received correctly due to direct feedthrough problem. Hence, first harmonic signal is filtered out in both hardware and software level. The effect of high-pass filtering signal results in a DC loss in image domain, since first harmonic signal corresponds to a constant in $U_0\left(\frac{2x}{W}\right)$ as can be seen in Figure 1.

$$\hat{\rho}_{lost}(x) = \alpha S_1 U_0\left(\frac{2x}{W}\right) = \alpha S_1 \tag{6}$$

This DC loss appears separately in each pFOV, and DC loss in each pFOV depends on the particle distribution on that pFOV.

(7)

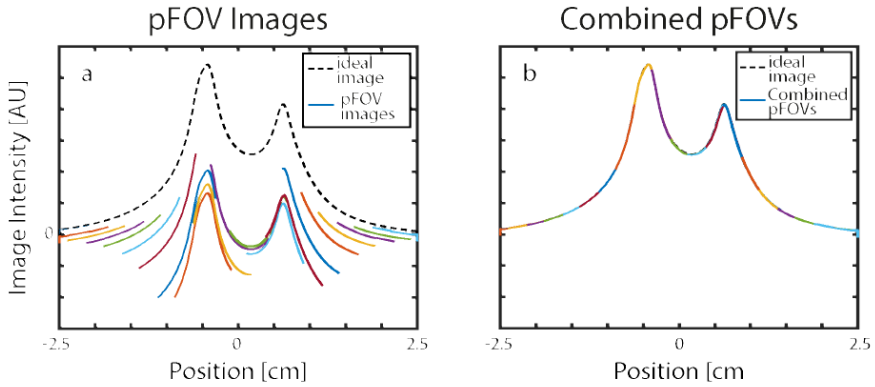

Fig. 2. Standard x-space reconstruction. (a) pFOV images having different DC losses due to high-pass filtering (b) Combining pFOV images by enforcing the smoothness and non-negativity [3]

1.2. Partial FOV Centering Imaging (PCI): A Robust X-Space Image Reconstruction for Magnetic Particle Imaging [4]

Image of entire FOV is obtained by combining all pFOVs, as shown in Figure 2, and this process may be sensitive to non-ideal signal conditions such as harmonic interference, noise and relaxation effects. Partial FOV Centering Imaging (PCI) is a novel robust x-space image reconstruction for MPI developed with the motivation of eliminating non-ideal effects on signal. There are two proposed methods, PCI and Lumped PCI. PCI and Lumped-PCI methods offer a trade-off between interference and noise robustness.

1.2.1. PCI [4]

PCI simply samples the centers of pFOVs, locates them closely by overlapping pFOVs and applies deconvolution to get rid of DC loss due to direct feedthrough filtering. Speed compensation is not necessary step in PCI as it is in x-space reconstruction, since instantaneous FFP speed at the center for all pFOVs are equal.

$$s(t) = \alpha \dot{x}_s(t) \hat{\rho}(x_s(t)) \tag{8}$$

$$\hat{\rho}\big(x_s(t)\big) = \rho(x) * h(x)\big|_{x = x_s(t)} \tag{9}$$

N is the total number of pFOVs, x_{0j} is the sample at the center of j^{th} pFOV.

$$x_s(t)\big|_{t=t_{0j}} = x_{0j}, \text{ for } j = 1, \dots, N \tag{10}$$

$$\begin{aligned}\hat{\rho}_0(x_{oj}) &= s(t)|_{\,t = t_{oj}} \\ &= \alpha \dot{x}_s(t_{0j})\hat{\rho}(x_{0j}) \\ &= \beta_0 \hat{\rho}(x_{0j})\ for\ j = 1, \dots, N\end{aligned} \tag{11}$$

$\hat{\rho}_{dc}(x)$ can be written as convolution operation by using symmetry property of $\sqrt{1-\left(\frac{2x}{W}\right)}$ from Eqn. 7 and $\hat{\rho}_{dc}(x)$ becomes result of convolution of particle distribution with DC kernel $\sqrt{1-\left(\frac{2x}{W}\right)}$.

$$\hat{\rho}_{dc}(x_{0j}) = \frac{4}{\pi W}\left(\hat{\rho}(x) * \sqrt{1-\left(\frac{2x}{W}\right)}\right)\Bigg|\, x = x_{0j} \tag{12}$$

$\tilde{\rho}_0(x)$ is the image with DC loss due to high-pass filtering first harmonic signal.

$$\tilde{\rho}_0(x_{0j}) = \beta_0\left(\hat{\rho}(x_{oj}) - \hat{\rho}_{dc}(x_{oj})\right) \tag{13}$$

$$\tilde{\rho}_0(x_{0j}) = \hat{\rho}(x) * h_0(x)|_{\,x = x_{0j}} \tag{14}$$

$$\tilde{\rho}_0(x) = \hat{\rho}(x) * h_0(x) \tag{15}$$

$$h_0(x) = \beta_0\left(\delta(x) - \frac{4}{\pi W}\sqrt{1-\left(\frac{2x}{W}\right)^2}\right) \tag{16}$$

$$\hat{\rho}(x) = \tilde{\rho}_0(x) *^{-1} h_0(x) \tag{17}$$

PCI is the deconvolution operation shown in Eqn. 17.

1.2.1. Lumped PCI [4]

N is the total number of pFOVs, and there are $2K + 1$ sampling positins in one pFOV.

$$x_s(t)|_{\,t = t_{kj}} = x_{kj}, for\ j = 1, \dots, N\ and\ k = -K, \dots, K \tag{18}$$

x_{kj} is the sample at k^{th} position of j^{th} pFOV. Samples at k^{th} positions are assigned to the centers. This assigning operation increases signal-to-noise ratio as more samples with the same noise distributions are taken for one point.

$$\hat{\rho}_k(x_{oj}) = \beta_k \hat{\rho}(x_{kj}) \tag{19}$$

$h_0(x)$ in Eqn. 16 can be modified accordingly:

$$h_k(x) = \beta_k \left(\delta\left(x - (x_{0j} - x_{kj})\right) - \frac{4}{\pi W} \sqrt{1 - \left(\frac{2x}{W}\right)^2} \right) \tag{20}$$

$\hat{\rho}(x)$ can be obtained by deconvolution of $\tilde{\rho}_k(x)$, which is the k^{th} raw image.

$$\hat{\rho}(x) = \tilde{\rho}_k(x) *^{-1} h_k(x) \tag{21}$$

To increase SNR, each raw image can be summed up and $\tilde{\rho}_{lum}(x)$ becomes the lumped image. This is the reason why Lumped PCI is more robust against noise.

$$\tilde{\rho}_{lum}(x) = \sum_{k=-K}^{K} \tilde{\rho}_k(x) \tag{22}$$

$$\tilde{\rho}_{lum}(x) = \hat{\rho}(x) * h_{lum}(x) \tag{23}$$

$h_{lum}(x)$ becomes summation of each kernel for k^{th} position.

$$h_{lum}(x) = \sum_{k=-K}^{K} h_k(x) \tag{24}$$

$$\hat{\rho}(x) = \tilde{\rho}_{lum}(x) *^{-1} h_{lum}(x) \tag{25}$$

Lumped PCI is again the deconvolution operation applied on the lumped image as shown in Eqn. 25.

In x-space reconstruction, DC loss has the remedy of combining pFOVs by enforcing the smoothness and non-negativity as shown in Figure 2. Global DC loss cannot be recovered with this technique, but image can be obtained by saving linear-shift invariance (LSI) property of MPI image reconstruction. This approach is affected by non-ideal signal conditions [4]. When there is noise at the edges, the combined pFOVs are shifted upwards cumulatively and this results in a stripe in x-space reconstruction image results which can be seen at 10 dB SNR level in Figure 4.

Lumped PCI has the advantage of recovering DC loss by a very nice and trivial solution. The solution is that one can choose the kernel to be odd function by assigning an additional α_k constant to $h_k{}'$s . Moreover, this type of kernels give better results in implementation because $h_{lum}(x)$ tends to go to zero as sample number increases and converges to continuous case.

Let us define β_k for x_k in all pFOVs. x_k is the k^{th} position in one pFOV.

$$\beta_k = \sqrt{1 - \left(\frac{2x_k}{W}\right)^2} \tag{26}$$

By substituting Eqn. 26 into Eqn. 20, $h_{lum}(x)$ can be derived as follows:

$$\begin{aligned} h_{lum}(x) &= \sum_{k=-K}^{K} h_k(x) \\ &= \sum_{k=-K}^{K} \beta_k \left(\delta\left(x - \left(x_{0j} - x_k\right)\right) - \frac{4}{\pi W}\sqrt{1 - \left(\frac{2x}{W}\right)^2} \right) \\ &= \sum_{k=-K}^{K} \sqrt{1 - \left(\frac{2x_k}{W}\right)^2} \left(\delta\left(x - (x_0 - x_k)\right) - \frac{4}{\pi W}\sqrt{1 - \left(\frac{2x}{W}\right)^2} \right) \end{aligned} \tag{27}$$

When sample number increases inside pFOV, discrete kernel converges to continuous function as in Eqn. 28.

$$\int_{-\frac{W}{2}}^{\frac{W}{2}} \sqrt{1 - \left(\frac{2x}{W}\right)^2}\, dx = \frac{\pi W}{4} \tag{28}$$

$$\sum_{k=-K}^{K} \sqrt{1 - \left(\frac{2x_k}{W}\right)^2} \approx \frac{\pi W}{4} \tag{29}$$

As a result, $h_{lum}(x)$ converges to zero.

$$h_{lum}(x) \approx 0 \tag{30}$$

This may seem as a disadvantage at first, but it is not and solves DC loss problem in a trivial way. If we choose α_k to be odd function as $\alpha_{-k} = -\alpha_k$, $h_{lum}(x)$ gets rid of DC loss kernel. Lumped-PCI results does not depend on high-pass filtering.

$$\tilde{\rho}_{lum}(x) = \sum_{k=-K}^{K} \alpha_k \tilde{\rho}_k(x) \tag{31}$$

$$\begin{aligned} h_{lum}(x) &= \sum_{k=-K}^{K} \alpha_k h_k(x) \\ &= \sum_{k=-K}^{K} \alpha_k \beta_k \delta\left(x - \left(x_{0j} - x_{kj}\right)\right) \end{aligned} \tag{32}$$

PCI works better with harmonic interference since it is sampling the signal only at the center and center is not affected with interference very much. Lumped PCI works better with noise since sampled signals in each pFOVs are collected and located at the center. When more samples are taken for one sample point, SNR increases.

Results for Standard X-Space Reconstruction, Lumped PCI and PCI are shown in Figure 3. Phantom is convolved with PSF and reconstructed image are compared with ideal PSF blurred MPI image.

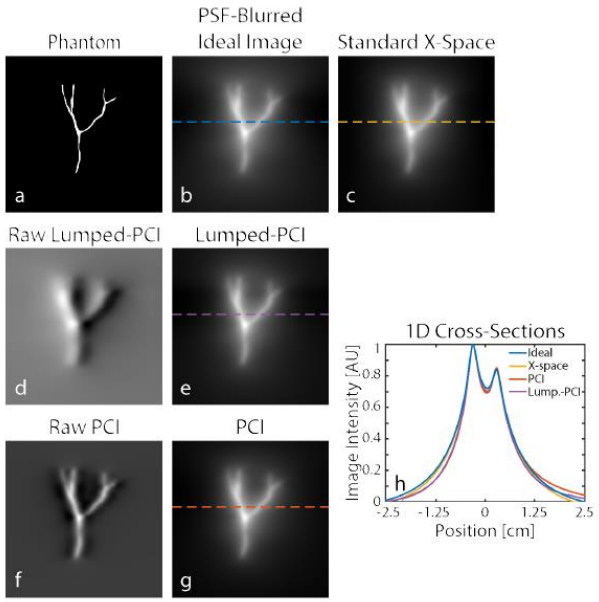

Fig. 3: Image Results for Standard X-Space Reconstruction, Lumped PCI and PCI

1.2.2. Noise and Harmonic Interference Robustness Analysis

Noise in simulations is added according to SNR definition in Eqn. 33 in simulations.

$$SNR = 20\log_{10}\left(\frac{\max_t |s(t))|}{\sigma}\right) \tag{33}$$

White Gaussian Noise is added on the signal $s(t)$ in time-domain and noises at each corresponding positions are independent and identically distributed (i.i.d.).

Harmonic interferences are added with respect to maximum Fourier coefficient value in the n^{th} harmonic bandwidth. $S_n(f)$ is the n^{th} harmonic band. SIR level at each harmonic band is the same.

$$SIR = 20\log_{10}\left(\frac{\max_f |S_n(f)|}{\gamma_n}\right) \tag{34}$$

$$S_n(f) = \begin{cases} S(f), & \left(n-\frac{1}{2}\right) f_0 < f < \left(n+\frac{1}{2}\right) f_0 \\ 0, & otherwise \end{cases} \tag{35}$$

$$f = nf_0$$

The magnitude of the interference at the n^{th} band is uniformly distributed between 0 and γ_n, and the phase is uniformly distributed between 0 and 2π. Randomness in phase results in a situation where no position in one pFOV is better-off. Therefore, the problem is limited to firstly constant phase, and then a Gaussian distribution with a centre mean value and small variance. This assumption was more suitable and realistic according to the observations in hardware. Randomness in magnitude is the same as before and modelled according to the observations of drifts in MPI scanner in the lab.

Results for noise and interference separately are shown in Figure 4 and 5. Throughout the project, the attempts to optimize noise and interference were implemented for separate case. After finding a method for noise and interference optimization, their combination will be studied.

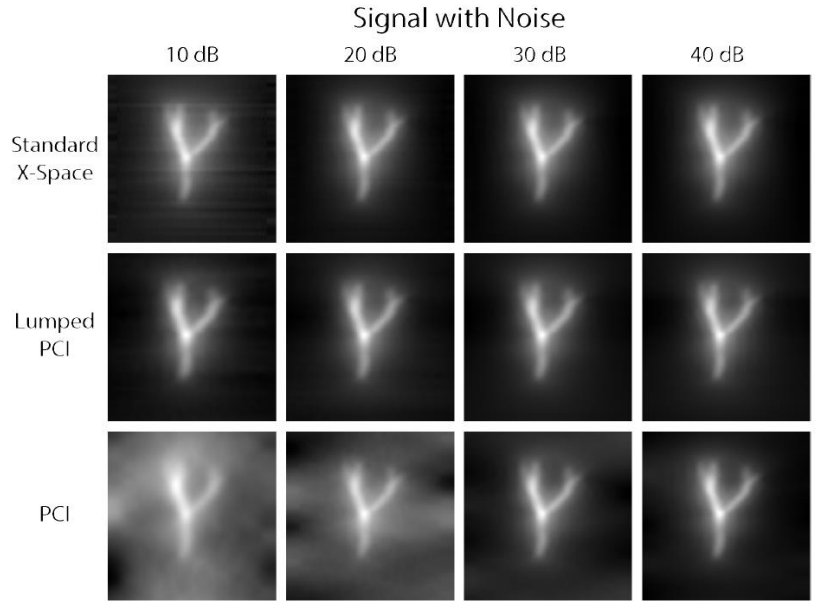

Fig. 4: Comparison of Standard X-Space Reconstruction, Lumped PCI and PCI Results at Different SNR levels [4]

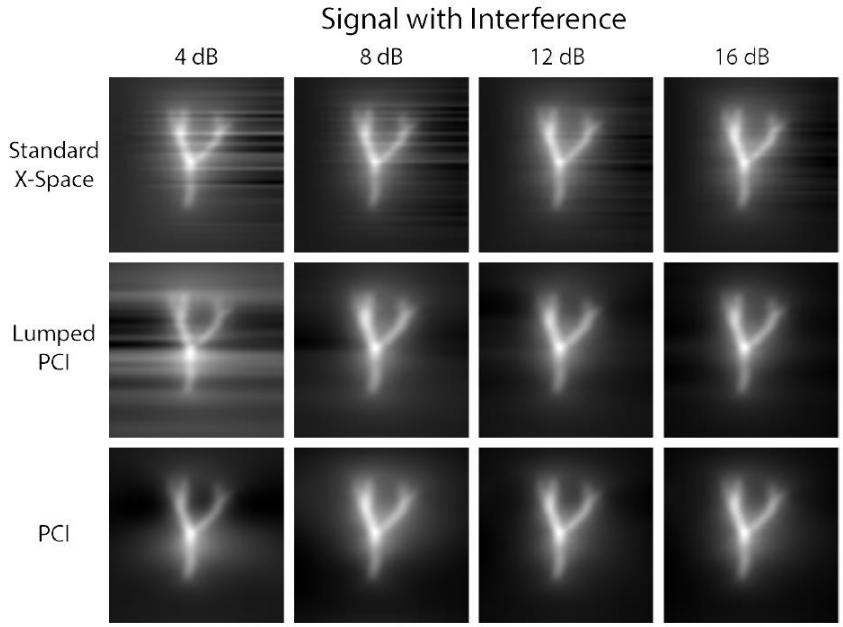

Fig. 5: Comparison of Standard X-Space Reconstruction, Lumped PCI and PCI Results at Different SIR levels [4]

2. Methods

2.1. Noise Robustness

2.1.1. Nosie Analysis

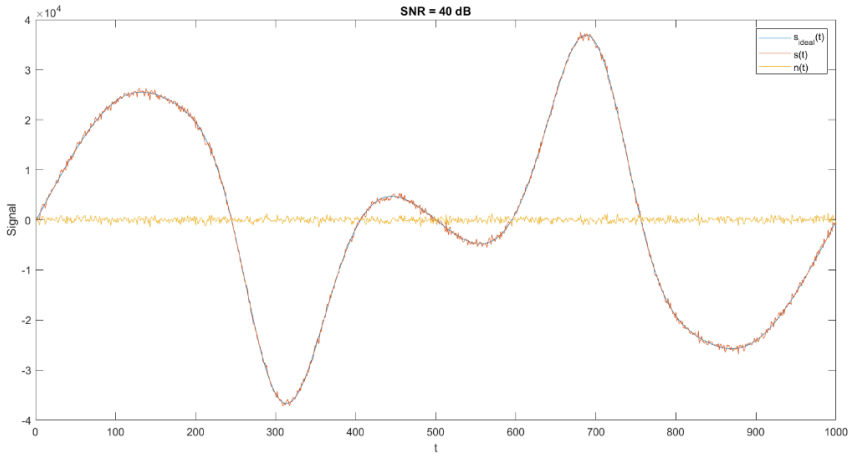

Fig. 6: Noise Profile in Middle Line (#26) and Middle pFOV (#291)

There are 51 horizontal lines and signal is taken in 1D by scanning each line separately. In each scanned line, there are 582 pFOVs and these pFOVs are overlapped Only positive cycle of pFOV signal is utilized in PCI and Lumped PCI simulations [3].

In Figure 6, displayed signal has full cycle with 1000 samples in time domain. Utilized samples are from 500 to 1000 in simulations. Displayed signal in Figure 6 has loss of first harmonic signal.

As stated before, i.i.d. white Gaussian noise, $n(t)$, is added on $s(t)$ at each time instance. Signal with noise becomes,

$$s(t) = s_{ideal}(t) + n(t) \tag{36}$$

In lumped PCI, firstly raw lumped-PCI imaqes for each sampling position are summed up as shown in Figure 3.d. Then, deconvolution operation is applied. Therefore, the proposed method for noise robustness is applied before raw-lumped PCI creation.

2.1.2. SNR Optimization for Lumped-PCI

SNR optimization for Lumped PCI is adapted from Signal-to-Noise Ratio Optimized Image Reconstruction Technique for MPI [4]. In standard x-space reconstruction, images in pFOVs are found separately by overlapping and overlapped images are averaged to obtain whole image in FOV by enforcing non-negativity and smoothness constraints. While averaging pFOV images, SNR is optimized when each position in pFOV images are weighted by the square of FFP speed before summation. Similarly, if we can find a weighting for SNR optimization of raw lumped-PCI image, we can increase noise robustness [4].

$\tilde{\rho}_k$ is the image with DC, n_k is the added i.i.d. white Gaussan noises, and c_k is the desired weighting coefficient for SNR optimization at the k^{th} position in one pFOV. There are $2K + 1$ positions in pFOVs. We want to optimize the SNR value of raw lumped image. Lumped image with noise is as follows:

$$\tilde{\rho}_{lum,ideal} = \sum_{k=-K}^{K} \beta_k \tilde{\rho}_k \, , where \; k = -K, \dots, K \tag{37}$$

$$\tilde{\rho}_{lum} = \sum_{k=-K}^{K} (\beta_k \tilde{\rho}_k + n_k) \tag{38}$$

$$\tilde{\rho}_{lum} = \sum_{k=-K}^{K} c_k (\beta_k \tilde{\rho}_k + n_k) \tag{39}$$

$$\tilde{\rho}_{lum} = \sum_{k=-K}^{K} c_k \beta_k \tilde{\rho}_k + \sum_{k=-K}^{K} c_k n_k \tag{40}$$

Our SNR definition for raw lumped image is as follows:

$$SNR = 20\log_{10}\left(\frac{|\sum_{k=-K}^{K} c_k\,\beta_k\tilde{\rho}_k|}{\sigma'}\right) \tag{41}$$

Noises at k^{th} positions are $n_k \sim N(0,\sigma^2)$ with same standard deviation σ. Standard deviation of raw lumped image for one pFOV becomes,

$$\sigma' = \sqrt{\sum_{k=-K}^{K} {c_k}^2\,\sigma^2} = \sigma\sqrt{\sum_{k=-K}^{K} {c_k}^2} \tag{42}$$

We want to optimize the SNR in Eqn. 41 by choosing right c_k coefficients for each positions, hence we take the derivative of SNR term with respect to c_j and set to zero for j^{th} position.

$$\frac{\partial}{\partial c_j}\left(\frac{\sum_{k=-K}^{K} c_k\beta_k\tilde{\rho}_k}{\sigma\sqrt{\sum_{k=-K}^{K} {c_k}^2}}\right) = \frac{\sigma\beta_j\tilde{\rho}_j\sqrt{\sum_{k=-K}^{K} {c_k}^2} - \sum_{k=-K}^{K} c_k\beta_k\tilde{\rho}_k\,.\left(\frac{1}{2\sqrt{\sum_{k=-K}^{K} {c_k}^2}}\,2\,c_j\,\sigma\right)}{\sigma^2\,\sum_{k=-K}^{K} {c_k}^2} \tag{43}$$

$$\beta_j\tilde{\rho}_j\sqrt{\sum_{k=-K}^{K} {c_k}^2} - \sum_{k=-K}^{K} c_k\beta_k\tilde{\rho}_k\,.\frac{c_j}{\sqrt{\sum_{k=-K}^{K} {c_k}^2}} = 0 \tag{44}$$

$$\beta_j\tilde{\rho}_j\sum_{k=-K}^{K} {c_k}^2 - \left(\sum_{k=-K}^{K} c_k\beta_k\tilde{\rho}_k\right).c_j = 0 \tag{45}$$

$$c_j = \beta_j\tilde{\rho}_j\frac{\sum_{k=-K}^{K} {c_k}^2}{\sum_{k=-K}^{K} c_k\beta_k\tilde{\rho}_k} \tag{46}$$

$\frac{\sum_{k=-K}^{K} {c_k}^2}{\sum_{k=-K}^{K} c_k\beta_k\tilde{\rho}_k}$ is a constant for each pFOV, then we can define a constant μ for this term.

$$\mu = \frac{\sum_{k=-K}^{K} {c_k}^2}{\sum_{k=-K}^{K} c_k\beta_k\tilde{\rho}_k} \tag{47}$$

$$c_j = \mu\beta_j\tilde{\rho}_j \tag{48}$$

We need to find one constant c_k for k^{th} position, since found c_k's will be substituted into Eqn. 39. Following this, $h_{lum}(x)$ will be multiplied for each k^{th} position by the new c_k

coefficient. It should not depend on $\tilde{\rho}_j$, hence $\tilde{\rho}_j$'s are assumed to be equal by assuming uniform particle distribution in pFOVs.

This result is intuitive since we trust center samples the most, and the edges the least due to speed compensation in x-space reconstruction [5]. There is no speed compensation in Lumped-PCI, but speed compensation is inherently implemented by deconvolution with $h_{lum}(x)$ kernel. When we multiply with instantaneous FFP speed, we weight centers the most, and suppress the edges. In results, there is a slight improvement in noise robustness, however Lumped PCI was not affected hugely by noise as it was in PCI and therefore more work focusing on interference robustness is needed to optimize Lumped PCI.

2.2. Interference Robustness

2.2.1. Interference Analysis

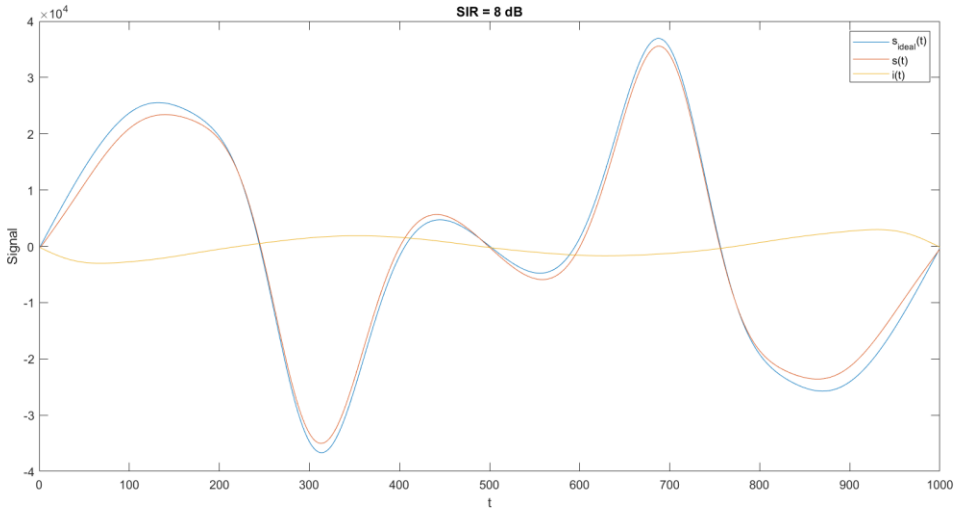

Fig.7: Interference Profile in Middle Line (#26) and Middle pFOV (#291)

Harmonic interference addition is seen in Figure 7 at the SIR level of 8 dB. We can model interference and ideal signal separately:

$$s(t) = s_{ideal}(t) + i(t) \tag{49}$$

We know that $s_{ideal}(t)$ is periodic as in Eqn. 4, harmonic interferences are added proportional to Fourier coefficients S_n.

$$s(t) = \sum_n S_n \sin(2\pi f_n t) + \sum_n I_n \sin(2\pi f_n t + \phi_n), \tag{50}$$

$$where\ I_n \sim U(0, \gamma_n)\ and\ \phi_n \sim U(0,2\pi)$$

Firstly, let us look at the expectance of interferencing signal for uniformly distributed random phase.

$$E[i(t)] = E\left[\sum_n I_n \sin(2\pi f_n t + \phi_n)\right] = \sum_n E[I_n]E[\sin(2\pi f_n t + \phi_n)] \quad (51)$$

Let us find $]E[\sin(2\pi f_n t + \phi_n)]$ in Eqn 51.

$$E[\sin(2\pi f_n t + \phi_n)] = \int_0^{2\pi} \frac{1}{2\pi} \sin(2\pi f_n t + \phi_n) d\phi_n = 0 \quad (52)$$

When phase is constant, expectance of interferencing signal becomes 0, which means none of the positions as better-off. Additionally, this is not realistic for hardware observations. Hence, firstly phase is assumed to be constant. Afterwards, we defined phase to be distributed in a small boundary as $\phi_n \sim N\left(0, \frac{\pi}{10}\right)$.

$$E\left[\sum_n I_n \sin(2\pi f_n t)\right] = \sum_n E[I_n]E[\sin(2\pi f_n t)] = \sum_n \sin(2\pi f_n t)\, E[N_n] = \sum_n \frac{\gamma_n}{2} \sin(2\pi f_n t) \quad (53)$$

Harmonic interference at n^{th} harmonics are shown in Fig. 8. By looking at Fig. 8, it can be better understood why PCI is robust for harmonic interference. When phase is constant, interference at the center becomes small. Also, harmonic interference at each pFOV is the same because of periodicity and relative image result is affected less by interference for having same signal addition at the centers for all pFOVs.

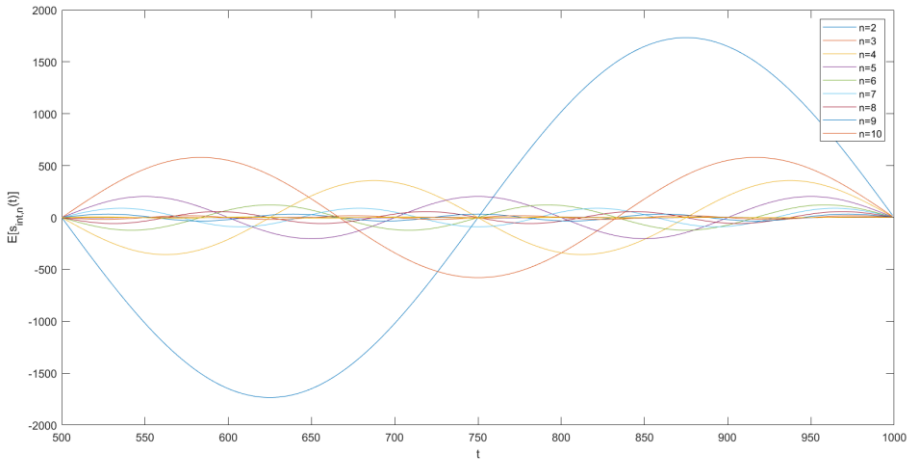

Fig. 8: Expectance of Harmonic Interferences at n^{th} Harmonics for Middle line

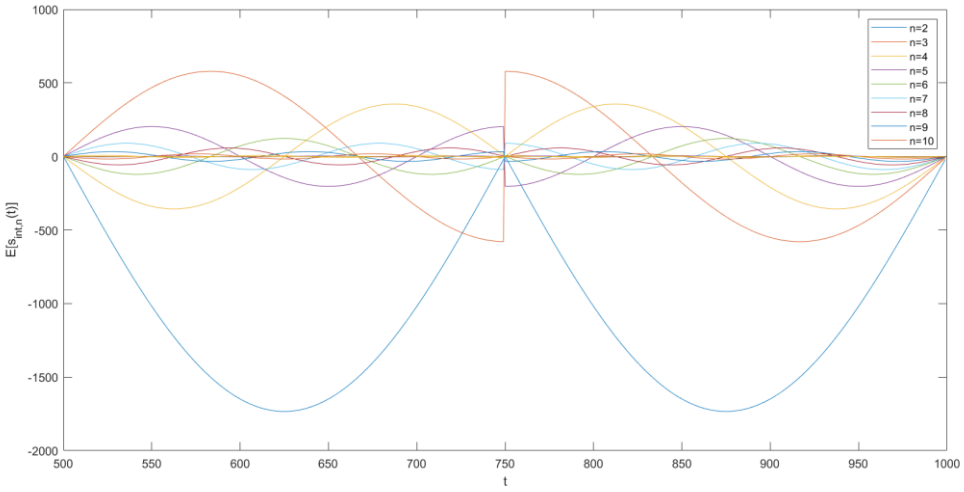

Fig. 9: Expectance of Harmonic Interferences at n^{th} Harmonics for Middle Line

(The sign of α_k's are included.)

In Figure 9, integration for n=3,4,5,7,8,9 are equal to zero, while integration for *n* =2,6,10 are not equal to zero. We can state that raw lumped-PCI image is affected by harmonic interference if the division of *n* by 2 is an odd number, then raw-lumped PCI will be affected by the harmonic interference. Again, α_k's being odd function is a remedy for harmonic interference to a certain level. We will try to optimize it even more. Here, we should keep in mind that phase is assumed to be constant for simplification of the problem as a first step.

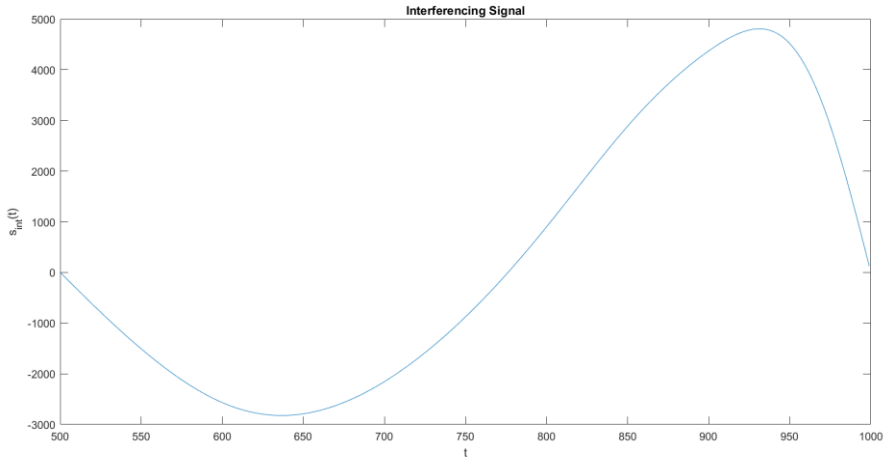

Fig. 10: Total Expectance of Harmonic Interferences at n^{th} Harmonics for Middle Line

In Figure 10, displayed harmonic interference is not symmetric whereas we have chosen α_k to be odd function before. This will be a challenge for optimizing interference robustness via finding a weighting strategy.

2.2.2. SNR Optimization Approach for Interference Robustness

Modeling harmonic interference as random noise in Eqn. 38 is considered as a solution for SIR optimization. This approach did not give good results because interference at different positions are not independent from each other, and their summation by raw lumped-PCI image creation should not be discarded for the problem. Therefore, searching for a solution by expectance of harmonic interference is a better solution way.

2.3. Kernel Optimization

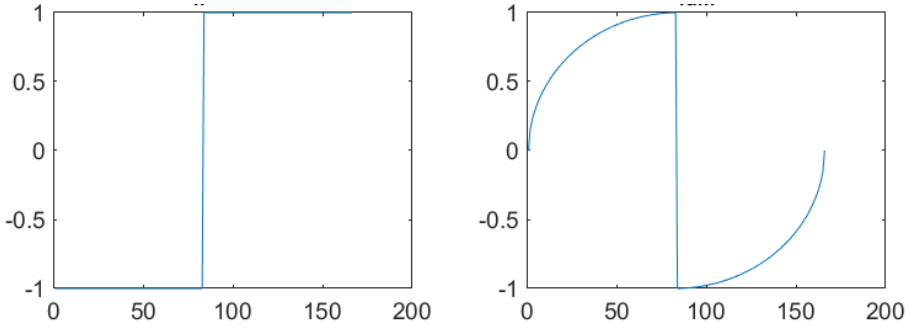

(a) (b)

Fig. 11: Deconvolution Kernels for Lumped-PCI,

(a) graph of k vs. α_k, (b) graph of x vs. $h_{lum}(x)$

There is a sharp transition in α_k and its results in a sharp transition in $h_{lum}(x)$. In our Lumped-PCI images, there are ringing artifacts, which may be resulting from this sharp transition. Bipolar sigmoid function in Eqn. 54 is used to smoothen this transition.

$$f(x) = \frac{1 - e^{-\lambda x}}{1 + e^{\lambda x}} \tag{54}$$

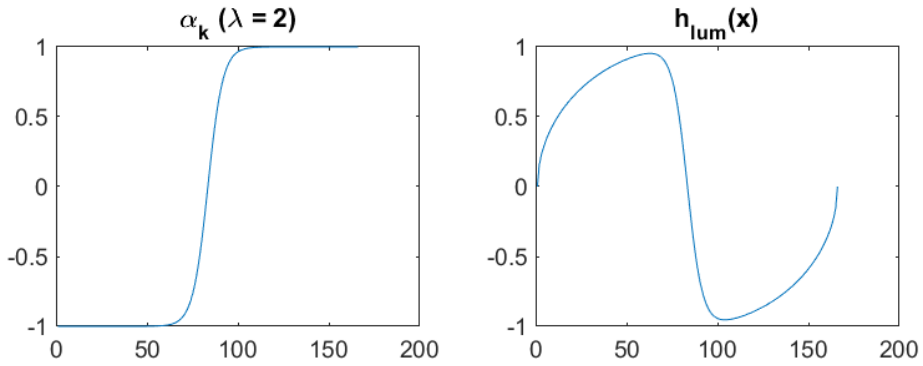

(a)

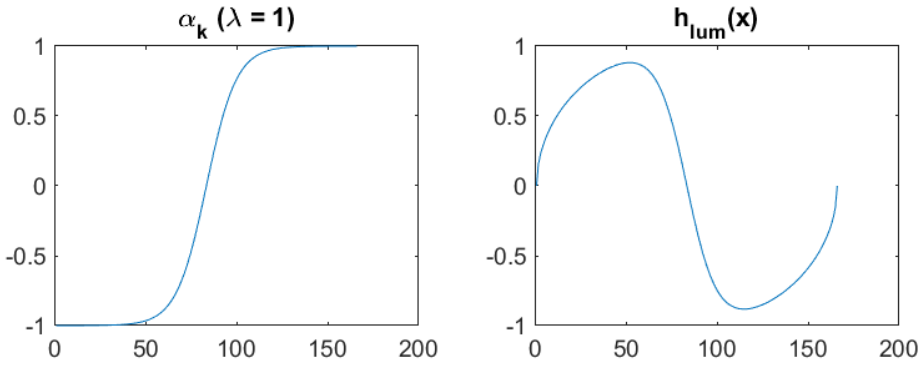

(b)

Fig. 12: α_k and $h_{lum}(x)$ after Smoothening by Bipolar Sigmoidal Function,

(a) $\lambda = 2$, (b) $\lambda = 1$

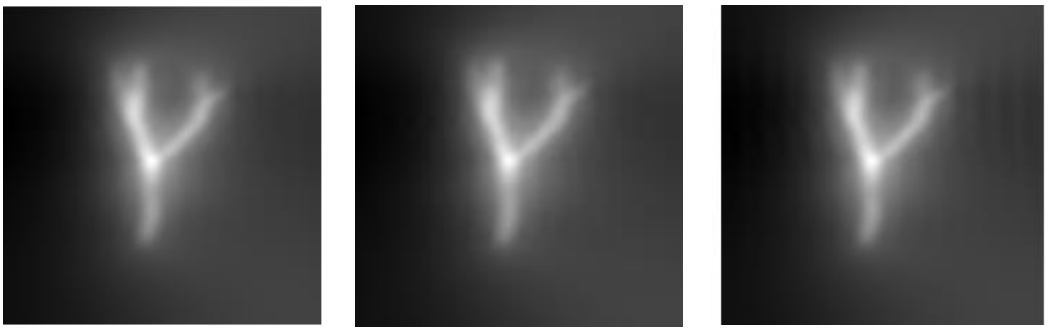

(a) (b) (c)

Fig. 13: Lumped PCI Result after Smooth Kernels, (a) regular kernel, (b) $\lambda = 2$, (b) $\lambda = 1$

Ringing artifacts did not vanish after smoothening kernels via bipolar sigmoid function. Tapering will be applied later for smoothening edges, since sharp decreases at the edges may be resulting in ringing artifacts, as well. α_k kernel might be multiplied by a Hanning window, and edges will go to zero smoothly.

3. Results

3.1. Results for SNR Optimization Technique for Noise Robustness

Improvements in images at 30 dB and 40 dB are not noticeable because lumped-PCI was already performing well for 30 dB and 40 dB SNR levels compared to 10 dB and 20 dB SNR levels. Improvement at 20 dB level is noticeable and noise around phantom is eliminated with good performance. At 10 dB SNR level, the improvements are noticeable and improvements are promising. However, the image gets more blurry, which raises the question that improvements may be resulting from deconvolution operation.

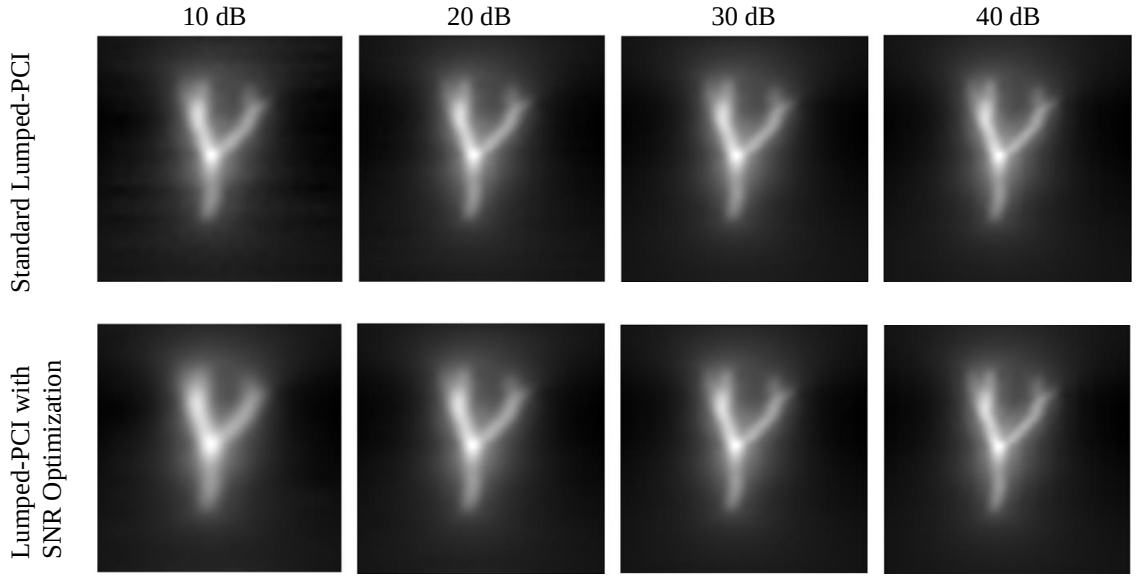

Fig. 14: Results of Lumped-PCI with SNR Optimization

In MATLAB, deconvolution operation for lumped-PCI is done by *deconvreg* function, and there is noise parameter for the function. It is required to tune the noise parameter, and results may be blurry for higher noise parameters. As an explanation, we may state that noise parameter for *deconvreg* was too high for the case that noise was reduced and therefore image became blurry since images do not get blurry at higher SNR levels. Still, this explanation is an intuitive explanation, since I do not know how exactly *deconvreg* functions.

3.2. Results for Interference Robustness

3.2.1. Interference Image Results

A method for interference robustness could not be developed yet. Results are shown to discuss about the nature of interference in Lumped-PCI**.**

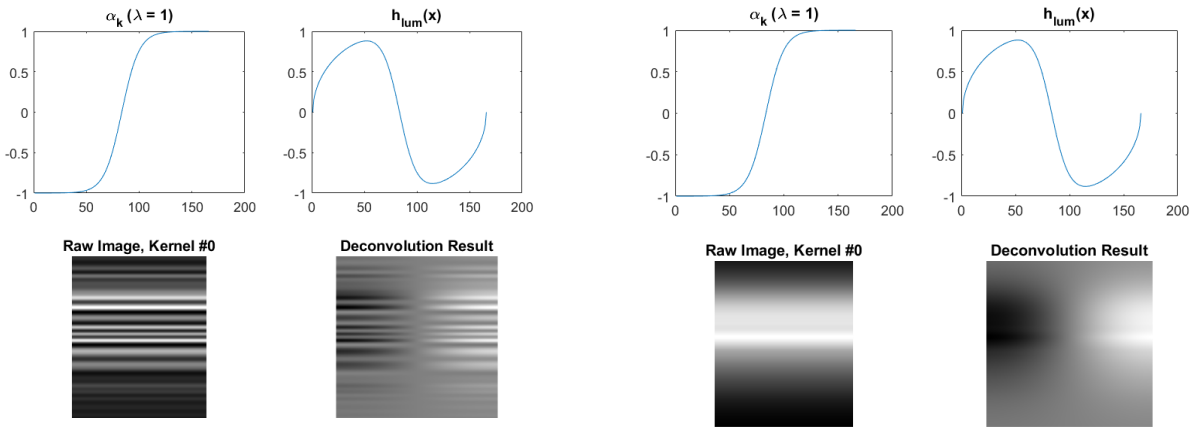

(a) (b)

Fig. 15: Image of Interference Signal $i(t) = \sum_n I_n \cos(2\pi f_n t + \phi_n)$, where $\phi_n = -\pi/2$ at 8 dB SIR level (a) the magnitude of harmonic interference signal is random $I_n \sim U(0, \gamma_n)$ for n^{th}harmonic, (b) the magnitude of harmonic interference signal is constant and $I_n = \gamma_n$

From Figure 15, interference image is not as expected. Since phase was constant and raw image is constant in horizontal axis, deconvolution result of Lumped-PCI was expected to be constant as well. Again, this raises the question how *deconvreg* functions and progress without understanding its functioning may be misleading.

3.2.2. Results for Different Kernel Trials at 4 dB SIR Level

Kernel #1 is the standard kernel used in Lumped-PCI technique. Kernel #2 is observed to see the SNR optimization for noise effect on image with interference. Kernel #3 was expected to be the worst result due to emphasis on edges, and results of Kernel #4 was expected to be the best result due to suppressing maximum interference positions. Image results have very slight changes, and some of the changes like in Kernel #3 result seems to be resulting from ringing artifacts. Therefore, before fixing the kernel by tapering, discussing results for interference does not make sense.

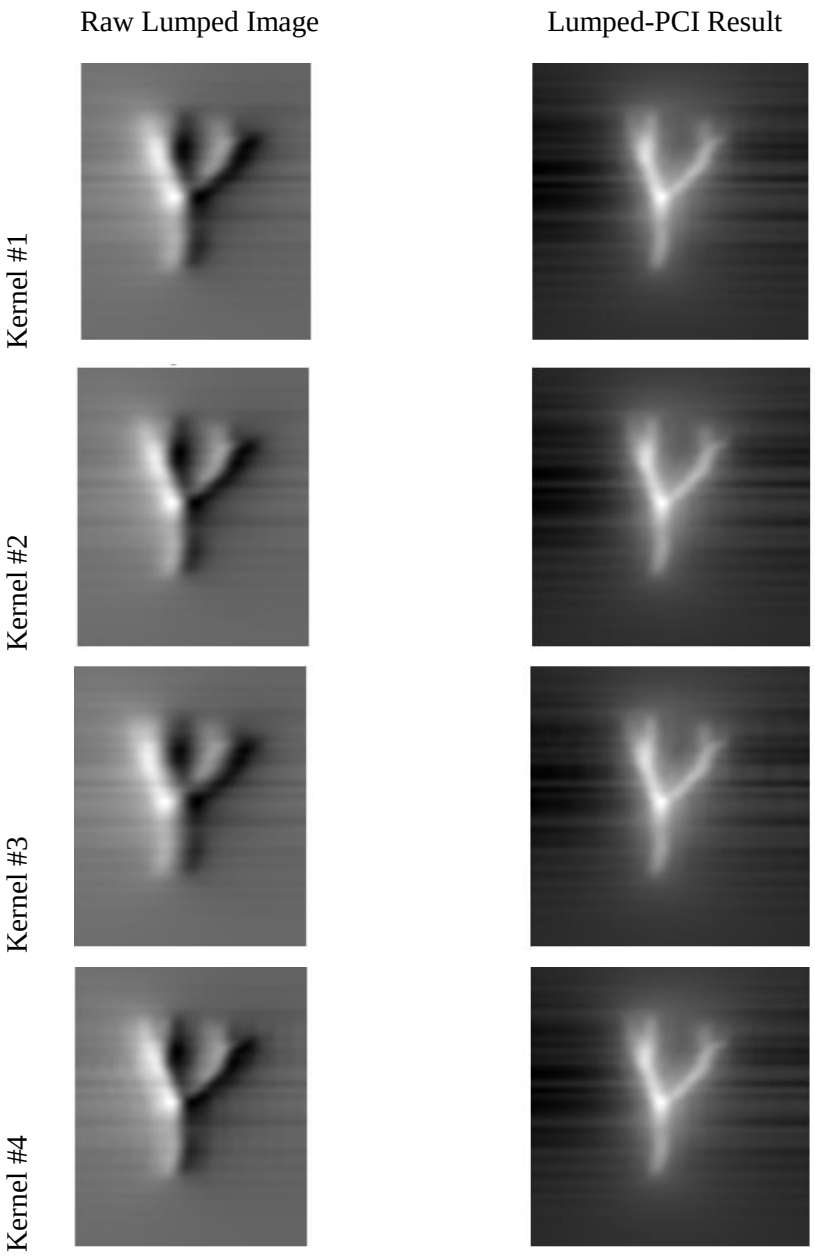

Fig.16:Lumped-PCI Results with Different Kernels

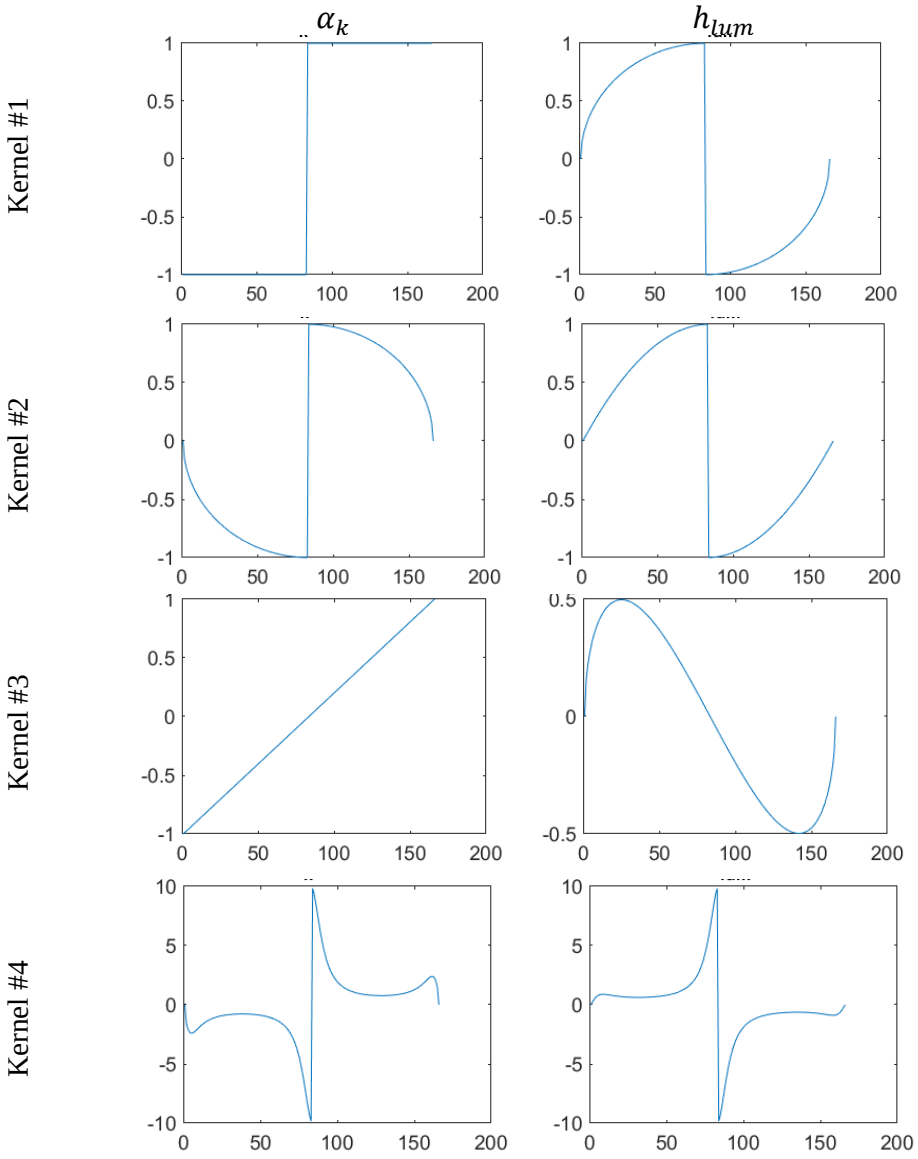

Fig. 17: Different Kernels for Lumped-PCI. Kernel #1 is standard kernel, Kernel #2 is the kernel used in SNR optimization technique, Kernel #3 is used for emphasising edges, and Kernel #4 is used for suppressing maximum interference positions.

4. Discussion

Noise robustness and interference robustness for Lumped-PCI method were studied in this project separately. For noise robustness, noise profile is analysed and the technique of SNR optimization in raw lumped-PCI image is developed. Lumped-PCI was already robust against noise, and its robustness was tried be increased even more. SNR optimization technique is also tried for the case with just interference, however image quality did not improve.

Several methods for interference robustness are tried, but a method could not be developed yet. Our first approach was to analyze variance of harmonic interference signal and weighting positions with high variance with lower coefficients before creating lumped-PCI image, effectively changing the kernel to suppress interference sensitive positions. However, our kernel has the property of being odd function and this gives us the advantage of eliminating harmonic interference at certain harmonics. Going from the expectance of harmonic interferences at each position and finding a weighting strategy for summing the harmonic interference expectation to be zero is going to be our next approach. Another approach may be using PCI image for Lumped-PCI image to increase interference robustness.

As future work, there are some problems to be fixed. Firstly, our kernel should be tapered and reference images should be taken at different SNR and SIR levels. Secondly, *deconvreg* function results should be understood better for understanding interference image results in Figure 15. Later, we will continue studying new approaches for interference robustness after fixing these problems.

References

[1] P. W. Goodwill and S. M. Conolly, “The x-space formulation of the magnetic particle imaging process: 1-D signal, resolution, bandwidth, SNR, SAR, and magnetostimulation,” *IEEE Transactions on Medical Imaging*, vol. 29, no. 11, pp. 1851–1859, 2010.

[2] K. Lu, P. W. Goodwill, E. U. Saritas, B. Zheng, and S. M. Conolly, “Linearity and shift invariance for quantitative magnetic particle imaging,” *IEEE Transactions on Medical Imaging*, vol. 32, no. 9, pp. 1565–1575, 2013.

[3] S. Kurt, “Rapid and Robust Image Reconstruction for magnetic Particle imaging,” M.S. Thesis, Grad. Sch. of Engineering and Science, Bilkent University, 2020.

[4] S. Kurt, Y. Muslu and E. U. Saritas, "Partial FOV Center Imaging (PCI): A Robust X-Space Image Reconstruction for Magnetic Particle Imaging," *in IEEE Transactions on Medical Imaging*, vol. 39, no. 11, pp. 3441-3450, Nov. 2020. doi: 10.1109/TMI.2020.2995410

[5] E. Bozkurt and E. U. Saritas, “Signal-to-noise ratio optimized image reconstruction technique for magnetic particle imaging,” *J. Fac. Eng. Archit. Gaz.*, vol. 32, pp. 999–1013, 2017.